

# Sensitivity of time-resolved diffraction data to changes in internuclear distances and atomic positions

Haeyun Jeong<sup>1</sup> | Hosung Ki<sup>1,2</sup> | Jong Goo Kim<sup>1,2</sup> | Jungmin Kim<sup>1,2</sup> |  
Yunbeom Lee<sup>1,2</sup> | Hyotcherl Ihee<sup>1,2</sup>

<sup>1</sup>Department of Chemistry and KI for the BioCentury, Korea Advanced Institute of Science and Technology (KAIST), Daejeon, Republic of Korea

<sup>2</sup>Center for Advanced Reaction Dynamics, Institute for Basic Science (IBS), Daejeon, Republic of Korea

## Correspondence

Hyotcherl Ihee, Department of Chemistry and KI for the BioCentury, Korea Advanced Institute of Science and Technology (KAIST), Daejeon, 34141, Republic of Korea.  
Email: hyotcherl.ihee@kaist.ac.kr

## Funding information

Institute for Basic Science, Grant/Award Number: R033

## Abstract

Time-resolved x-ray liquidography (TRXL) is a powerful technique to study molecular structural dynamics in the solution phase. Typically, a TRXL experiment is conducted during limited beamtime at a beamline of a synchrotron or an x-ray free-electron laser, demanding a proper design and careful planning. In this regard, the optimal  $q$  range needs to be determined to find the optimal x-ray energy and sample-to-detector distance. For such purpose, here, we present effective ways to quantify the sensitivity of the TRXL data as a function of  $q$  to various factors such as the atomic positions, internuclear distances, solvent cage, and bulk solvent. The developed approaches are also applicable to other types of time-resolved diffraction, such as ultrafast electron diffraction.

## KEYWORDS

data analysis, liquidography, sensitivity plot, structural dynamics, time-resolved diffraction, x-ray scattering

## INTRODUCTION

Time-resolved diffraction with x-ray or electron pulses is a powerful method that can provide direct structural information of reaction intermediates. Depending on the phase of the sample (gas, solid, and liquid phases) and the identity of the probe pulse (x-ray and electron), various versions of time-resolved diffraction techniques have been developed. Among them, time-resolved x-ray liquidography (TRXL), also known as time-resolved x-ray solution scattering, has been established as a useful method in studying the structural dynamics and kinetics of chemical and biological reactions in the liquid solution phase.<sup>1–86</sup> In a typical experiment of TRXL, an ultrashort optical pulse from a femtosecond laser system is used to initiate a reaction of interest, and an x-ray pulse with a time delay with respect to the laser pulse is used as the probe pulse to interrogate the status of the reaction progress.<sup>1–4</sup> X-ray scattering pattern is collected as a function of time delay between the pump pulse and the x-ray pulse. The scattering pattern can be expressed as a mathematical function of structural parameters such as bond lengths and angles. Thus, analyzing the scattering pattern can unveil the structural information,<sup>87–88</sup> and analyzing

the time-resolved scattering patterns can unveil the time-dependent structural changes of molecules.<sup>1–86</sup>

A TRXL experiment is conducted at a beamline of a synchrotron<sup>5–66</sup> or an x-ray free-electron laser (XFEL),<sup>67–76,89–90</sup> which provides x-ray pulses with a pulse width of  $\sim 100$  ps and  $\sim 100$  fs, respectively. Generally, beamtimes are offered based on competitive selection procedures of research proposals. Successful proposals, therefore, require careful design and planning. It is ideal that for a target molecule and the reaction of interest, the expected signal and noise are estimated to ensure that a satisfactory TRXL signal can be obtained in given beamtime and available experimental setups of the beamline. For this purpose, a program named *S-cube* was developed by our group.<sup>91</sup> The expected signal and noise for a given molecule and reaction can be estimated using *S-cube*. A typical TRXL signal has three components: (i) the solute-only term, (ii) the solute–solvent cross term (or cage term), and (iii) the solvent-only term (or solvent heating term).<sup>1–4</sup> *S-cube* also provides the expected noise level as well as the expected signal for each term, and thus the relative magnitudes of the three terms can be easily accessed.<sup>91</sup>

Besides these features, it would be ideal if two additional pieces of information are available in advance:

(i) how sensitively the difference scattering curve depends on the expected structural change as a function of  $q$ , and (ii) how sensitively the difference scattering curve changes with respect to various factors such as the atomic positions, internuclear distances, solvent cage, and bulk solvent that affect the difference scattering curves. In general, a larger  $q$  range for the difference curve is desirable because the structural resolution would be proportional to the  $q$  range. However, for a given beamline, the x-ray energy, which determines the x-ray wavelength, has a limited range, and the number of x-ray photons per pulse sensitively depends on the x-ray energy used for the TRXL experiment. Moreover, the sizes of the available detectors and the x-ray energy-dependent sensitivities of the detectors are generally fixed. With the larger x-ray energy, the smaller x-ray wavelength can give the larger range of  $q$  for a given detector size and a sample-to-detector distance. Usually, the x-ray energy can be tuned up to a certain limit, but at the expense of the number of x-ray photons. For this reason, the optimal x-ray energy and the sample-to-detector distance need to be chosen for the best use of the beamtime. For this purpose, the sensitivity of the difference scattering curve on the structural change associated with the expected reaction needs to be calculated as a function of  $q$ . Such information will identify the  $q$  range that is sensitive enough to capture the structural change of interest and thus will aid in determining an optimal  $q$  range for the experiment. In this work, we present a systematic way to quantitatively represent such information.

Another useful information is how sensitively the difference scattering curve changes with regard to the changes of the atomic positions and internuclear distances of the reactant and product molecules.<sup>4</sup> The TRXL signal is affected by diverse factors. For example, the change of the three-dimensional structure of reactant and product molecules contributes to the TRXL signal. In addition to the change of the molecules directly involved in the reaction, the change of the solvent cage surrounding the solute molecules and the change of bulk solvent due to the heating also affect the TRXL signal. In this regard, another useful piece of information is how sensitively the difference scattering curve changes with regard to the changes of these factors. For instance, for the reactant and product molecules, the TRXL signal can be expressed as a function of the parameters, including the positions of constituent atoms or the internuclear distances in the molecule. If one can predict which atomic positions or internuclear distances will contribute to the TRXL signal predominantly or if one can assess how much the solvent cage and the solvent heating will contribute to the TRXL signal, one can estimate the plausibility and applicability of TRXL in studying the structural dynamics of the molecule of interest before conducting an experiment. This work presents a protocol to visually display such information along with the sensitivities to the atomic positions, internuclear distances, solvent cage,

and solvent heating. This new feature will be implemented in the *S-cube* program.<sup>91</sup>

## TRXL data

From a TRXL experiment, two-dimensional (2D) scattering images are obtained as a function of time. Then, one-dimensional (1D) scattering curves,  $S(q, t)$ , are obtained by azimuthal integration of the 2D scattering images as a function of the momentum transfer  $q = (4\pi/\lambda)\sin(\theta)$ , where  $\lambda$  is the wavelength of x-rays,  $2\theta$  is the scattering angle, and  $t$  is the time delay between the laser and x-ray pulses.<sup>1–4</sup> The difference scattering curves,  $q\Delta S(q, t)$ , are obtained by subtracting  $S(q, t)$  at a negative time delay from  $S(q, t)$  at positive time delays and multiplying  $q$  to amplify the intensities at high scattering angle.

To analyze  $\Delta S(q, t)$  obtained from a TRXL experiment, one needs to calculate a theoretical  $\Delta S(q, t)$  curve. Usually, a theoretical  $\Delta S(q, t)$  with the following three components is considered.<sup>1–4</sup>

$$\Delta S(q, t) = \Delta S_{\text{solute}}(q, t) + \Delta S_{\text{cage}}(q, t) + \Delta S_{\text{solvent}}(q, t) \quad (1)$$

The solute-only term,  $\Delta S_{\text{solute}}(q, t)$ , contains information about the change of molecular structure of solute molecules, whose concentration changes with time according to the governing kinetics. The solute–solvent cross term (cage term),  $\Delta S_{\text{cage}}(q, t)$ , contains information about the change of the cage structure, which is coupled with the change of molecular structure of solute molecules. The solvent-only term,  $\Delta S_{\text{solvent}}(q, t)$ , is caused by the change of solvent temperature and density, which are also energetically linked to the kinetics of solute molecules because the heat released from the reaction of solute molecules governs the change of the temperature and density of solvent. Usually, the goal of data analysis is to determine the kinetic parameters and structures of solute molecules (reactants, intermediates, and products) that yield theoretical  $\Delta S(q, t)$  as close to the experimental  $\Delta S(q, t)$  as possible. For that purpose, theoretical  $\Delta S(q, t)$  is estimated with varying the kinetic parameters and structures of solute molecules and is compared with  $\Delta S(q, t)$ .

To calculate  $\Delta S(q, t)$ , first, one needs to calculate the solute-related term comprising the solute-only term and the cage term needs to be calculated. The solute-only term is calculated using the Debye equation. It should be noted that we used the form-factor parameterization introduced by Waasmaier and Krifel to calculate the solute-related term.<sup>92</sup> The cage term is obtained using MD simulations. From an MD simulation, a series of MD snapshots are obtained and used to calculate pair distribution functions,  $g(r)$ . The  $g(r)$  for a certain pair of atoms is then used to calculate the corresponding  $S(q)$  component. Depending on the atoms constituting the pair,

appropriate  $S(q)$ 's are used to calculate the cage term. The solvent-only term can be expressed as follows:

$$\Delta S(q, t)_{\text{solvent}} = \Delta T(t) \times (\partial S / \partial T)_\rho + \Delta \rho(t) \times (\partial S / \partial \rho)_T \quad (2)$$

where  $(\partial S / \partial T)_\rho$  is the change of the solvent scattering intensity in response to a temperature change at a constant density,  $(\partial S / \partial \rho)_T$  is the change of the solvent scattering intensity in response to a density change at a constant temperature, and  $\Delta T(t)$  and  $\Delta \rho(t)$  are the time-dependent changes in the temperature and density of the solvent, respectively. The two basis differentials,  $(\partial S / \partial T)_\rho$  and  $(\partial S / \partial \rho)_T$ , can be obtained either via MD simulations or in a separate solvent heating experiment using a dye solution.<sup>93</sup> The latter method gives more accurate differentials, whereas the former method is useful in assigning peak positions to specific atomic pairs.

### $q\Delta Z(q)$ : Metric to represent the sensitivity of $q\Delta S(q)$ to the structural change as a function of $q$

To check how sensitively  $q\Delta S(q)$  changes with the structural change, one can first calculate  $q\Delta S(q)$ 's for a range of structural changes for a given target reaction and check how the calculated  $q\Delta S(q)$ 's vary as a function of  $q$ . As a measure to quantitatively display the "sensitivity" of the TRXL signal to the structural change of the reactants and products, we propose to use the standard deviation. More specifically, the standard deviation of the several TRXL curves calculated with varying a structural parameter directly shows how much the signal is affected by the change of the structural parameter. In other words, the more sensitive the TRXL signal to a specific structural parameter, the TRXL signal would change more severely upon the change of the parameter. Accordingly, we propose that the standard deviation quantitatively represents the degree of the sensitivity of the TRXL signal and define the measure of the sensitivity using the equation for the standard deviation. With this approach, to quantify the sensitivity of  $q\Delta S(q)$  to the structural parameter, we introduce  $q\Delta Z(q)$ , which is the standard deviation of  $q\Delta S_i(q)$  calculated for various structures, as in the following equation:

$$q\Delta Z(q) = \sqrt{\frac{1}{N-1} \sum_{i=1}^N (q\Delta S_i(q) - q\Delta S_{\text{ave}}(q))^2} \quad (3)$$

Here,  $N$  is the total number of the difference scattering curves ( $q\Delta S_i(q)$ ) calculated for various structures,  $i = 1, 2, \dots, N$ , which differ in the structural parameter, and  $\Delta S_{\text{ave}}(q)$  is the average of  $\Delta S_i(q)$  as in the following equation:

$$\Delta S_{\text{ave}}(q) = \frac{1}{N} \sum_{i=1}^N \Delta S_i(q) \quad (4)$$

## RESULTS AND DISCUSSION

### $q\Delta Z(q)$ for the structural change as a function of $q$ : Gas-phase reactions

Prior to calculating  $q\Delta Z(q)$  through Equation (3), it is necessary to define a quantitative means to generate  $N$  structures which differ in the structural parameter. For example, we can consider the dissociation of a homonuclear diatomic molecule  $X_2$  into  $2X$  ( $X_2 \rightarrow X + X$ ) in the gas phase as a model reaction where the bond length  $R(X-X)$  of  $X_2$  is the structural parameter of interest. To inspect the sensitivity of the TRXL signal to  $R(X-X)$ ,  $q\Delta S(q)$ 's should be calculated for various structures of  $X_2$  having different  $R(X-X)$ . Here, it should be noted that the standard deviation of the  $q\Delta S(q)$ 's,  $q\Delta Z(q)$ , would vary depending on  $R(X-X)$ 's from which the  $q\Delta S(q)$ 's are calculated. Figure 1a shows  $q\Delta S(q)$ 's for the reaction  $I_2 \rightarrow I + I$  calculated for various  $R(I-I)$ 's ranging from 1.0 Å to 4.0 Å. The frequency of the oscillatory features increases with  $R(I-I)$  because of the reciprocal relation between the real space and the  $q$  space. Due to the change of the frequency of the oscillatory feature,  $q\Delta Z(q)$  significantly vary depending on both the value of  $R(I-I)$  around which the  $R(I-I)$ 's are sampled and the interval between the sampled  $R(I-I)$ 's.

One of the most straightforward ways to check whether  $R(X-X)$  is sensitive in the TRXL signal is to see whether there is a noticeable change in  $q\Delta S(q)$  when  $R(X-X)$  is increased or decreased from a certain value. Considering this, we generated three different structures with varying the internuclear distance by  $+\Delta r$ , 0, and  $-\Delta r$  from a certain value of  $R(X-X)$ . Figure 1b,c shows  $q\Delta Z(q)$  of  $I_2 \rightarrow I + I$  calculated for various  $R(X-X)$  values (Figure 1b) and intervals, or structural variance,  $\Delta r$  (Figure 1c). We also changed  $X$  to another atom and repeated the same calculations. Figure 1d compares the plots of  $q\Delta Z(q)$  for various types of atoms (iodine, chlorine, carbon, and hydrogen). These plots show that the sensitivity of the TRXL signal at the high  $q$  region increases rather dramatically with the atomic number of  $X$ . This result is well expected from how the x-ray atomic form factors depend on atoms. This result underscores the advantage of heavier atoms in terms of sensitivity and also shows that the scattering data at the high  $q$  region are more drastically benefited by molecules with heavier atoms.

As the second model reaction, we consider the structural change of  $X_2$  ( $X-X \rightarrow X-X$ ), where  $X = H, C, Cl$ , and  $I$ . The  $R(X-X)$  of the reactant was fixed at 2.5 Å, and  $R(X-X)$  was varied from 1.0 Å to 5 Å. Figure 1e shows  $q\Delta S(q)$  when  $X = I$ , and Figure 1f shows  $q\Delta Z(q)$  for various atoms with  $R(X-X) = 5$  Å.  $\Delta r$  for  $R(X-X)$  was set to be 0.1 Å. The plot of  $q\Delta Z(q)$  visualizes that the sensitivity of  $q\Delta S(q)$

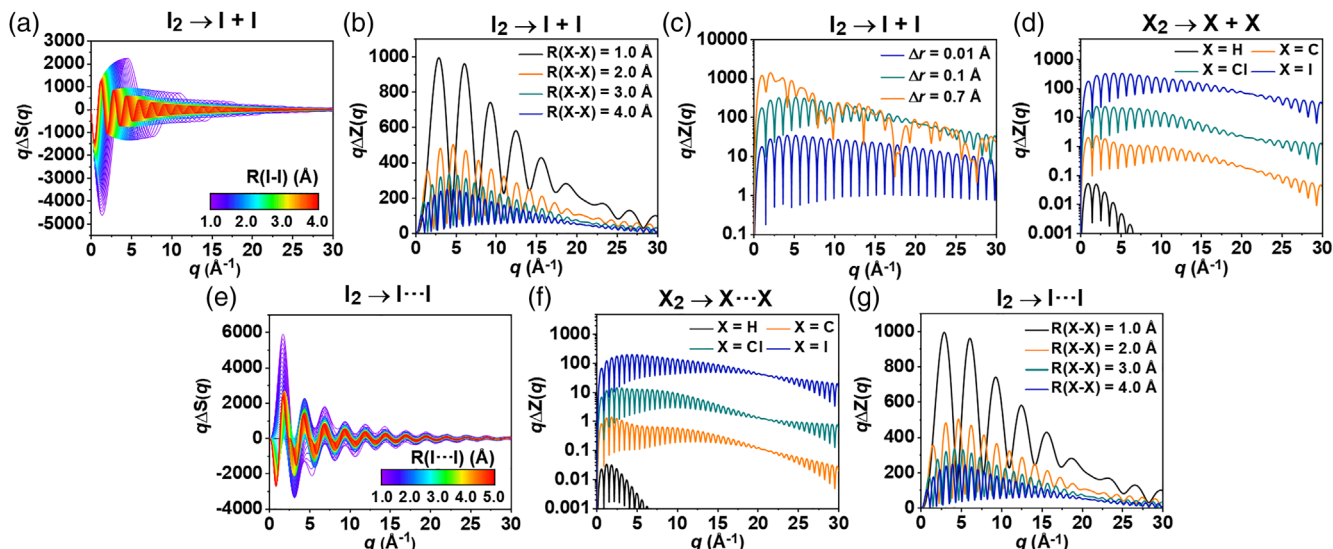


**FIGURE 1**  $q\Delta S(q)$  and  $q\Delta Z(q)$  for two simple gas-phase reactions: (a–d)  $X_2 \rightarrow X + X$  and (e–g)  $X \rightarrow X \cdots X$ . (a)  $q\Delta S(q)$  for  $X_2 \rightarrow X + X$  in the gas phase. Iodine atoms were used for X and the  $R(X-X)$  was varied from 1.0 Å to 4.0 Å. (b)  $q\Delta Z(q)$ , corresponding to  $R(X-X) = 1.0, 2.0, 3.0,$  and  $4.0$  Å, respectively.  $\Delta r = 0.1$  Å for  $R(X-X)$  is used to calculate  $q\Delta Z(q)$ . (c)  $q\Delta Z(q)$  corresponding to  $R(X-X) = 3.0$  Å with various values of  $\Delta r$ .  $\Delta r = 0.01, 0.1,$  and  $0.7$  Å for the  $R(X-X)$  are used to calculate  $q\Delta Z(q)$ , respectively. Plots (b) and (c) show that  $q\Delta Z(q)$  is dependent on the value of  $R(X-X)$  and  $\Delta r$ . (d)  $q\Delta Z(q)$  for various types of atoms ( $X = H, C, Cl,$  and  $I$ ) calculated for  $R(X-X) = 3.0$  Å with  $\Delta r = 0.1$  Å. (e)  $q\Delta S(q)$  for the structural change of  $X_2$  ( $X \rightarrow X \cdots X$ ) in the gas phase, where  $X = I$ . The  $R(X-X)$  of the reactant is fixed at 2.5 Å and the  $R(X \cdots X)$  is varied from 1.0 Å to 5.0 Å. (f)  $q\Delta Z(q)$  for  $R(X-X)$  of the reaction  $X \rightarrow X \cdots X$  for various types of atoms ( $X = H, C, Cl,$  and  $I$ ).  $q\Delta Z(q)$  is calculated for  $R(X \cdots X) = 5.0$  Å with  $\Delta r = 0.1$  Å. The  $R(X-X)$  of the reactant is fixed at 2.5 Å. (g)  $q\Delta Z(q)$  for  $R(X-X)$  of the reaction  $X \rightarrow X \cdots X$ , corresponding to  $R(X-X) = 1.0, 2.0, 3.0,$  and  $4.0$  Å, respectively, with  $\Delta r = 0.1$  Å. Iodine atoms are used for X and the  $R(X \cdots X)$  is fixed at 5.0 Å for the calculation of  $q\Delta Z(q)$ .

to the structural parameter of  $R(X \cdots X)$  decreases with  $q$  but increases at the high  $q$  region dramatically with the atomic number of X. This feature is quite similar to the case of Figure 1b–d.

To demonstrate the calculations of  $q\Delta Z(q)$  for larger molecules composed of several atoms, we then consider the dissociation of  $C_n$  into  $C_{n-1} + C$  ( $C_n \rightarrow C_{n-1} + C$ ). For simplicity,  $C_n$  and  $C_{n-1}$  are set to have linear structures with the same  $R(C-C)$  for all nearest  $C-C$  pairs except for  $R(C \cdots C)$  for the dissociating terminal  $C \cdots C$  pair in  $C_n$ . To calculate  $q\Delta Z(q)$  for the  $R(C \cdots C)$  of the dissociating  $C \cdots C$  pair, the structure of  $C_n$  is modified by changing the  $R(C \cdots C)$  by  $\Delta r$  from the equilibrium distance, while the other internuclear distances are fixed to the reference distances. In general, when there are  $N$  interatomic distances in a molecule, it is impossible to change only one distance without affecting the other  $N-1$  distances. Here, however, when estimating the sensitivity to a specific bond distance,  $R(C \cdots C)$ , we assumed such an impossible, unrealistic case; we changed the specific bond distance while the other bond distances were maintained. We used this approach for the following reason. If we consider a realistic structural change, multiple structural parameters are correlated so that even if one tries to change only one parameter, several parameters are changed simultaneously.  $q\Delta Z(q)$  calculated for such a structural change, where several parameters change all together, may not accurately describe the sensitivity to the change of a specific structural parameter.

The  $q\Delta S(q)$  for  $R(C \cdots C)$  of the dissociating  $C \cdots C$  bond in  $C_n$  from 1.0 Å to 4.0 Å are calculated (Figure 2a), and  $q\Delta Z(q)$  is shown for four different  $R(C \cdots C)$ 's with  $\Delta r = 0.1$  Å in Figure 2b. Then, the size of the molecule,  $n$ , was scanned from  $n = 2$  to  $n = 30$ , and the result is plotted together in Figure 2c. This plot reveals that  $q\Delta Z(q)$  does not depend on the size of the molecule. Subsequently, we repeated the same calculation for the case where C is replaced with H, Cl, and I, with  $n$  fixed at 20, and the results are shown in Figure 2d. The plots of  $q\Delta Z(q)$  in Figure 2d show the same trend observed in the first model reaction shown in Figure 1d.

Here, it should be noted that  $q\Delta Z(q)$  in Figure 1b–d,f visualizes the sensitivity to only a single structural parameter,  $R(X-X)$  and  $R(X \cdots X)$ , respectively. In the same way, Figure 2b represents the sensitivity to only a single structural parameter of  $R(C \cdots C)$ . For the reaction of  $X_2 \rightarrow X + X$ ,  $q\Delta Z(q)$  for a single structural parameter is enough. On the contrary, the reaction of  $X \rightarrow X \cdots X$  has two structural parameters,  $R(X-X)$  and  $R(X \cdots X)$ , and thus  $q\Delta Z(q)$  for a single structural parameter is not enough. In this case, to quantify the sensitivity to  $R(X-X)$  instead of  $R(X \cdots X)$ ,  $q\Delta Z(q)$  needs to be calculated for  $R(X-X)$ . For this purpose, we also estimated  $q\Delta Z(q)$  for  $R(X-X) = 2.5$  Å with  $\Delta r = 0.1$  Å where  $R(X \cdots X)$  was fixed at 5 Å. Figure 1g shows the corresponding  $q\Delta Z(q)$ . At this point, naturally, we consider a method to visualize the sensitivities to multiple structural parameters simultaneously. For this reason, we devised such a method described in the

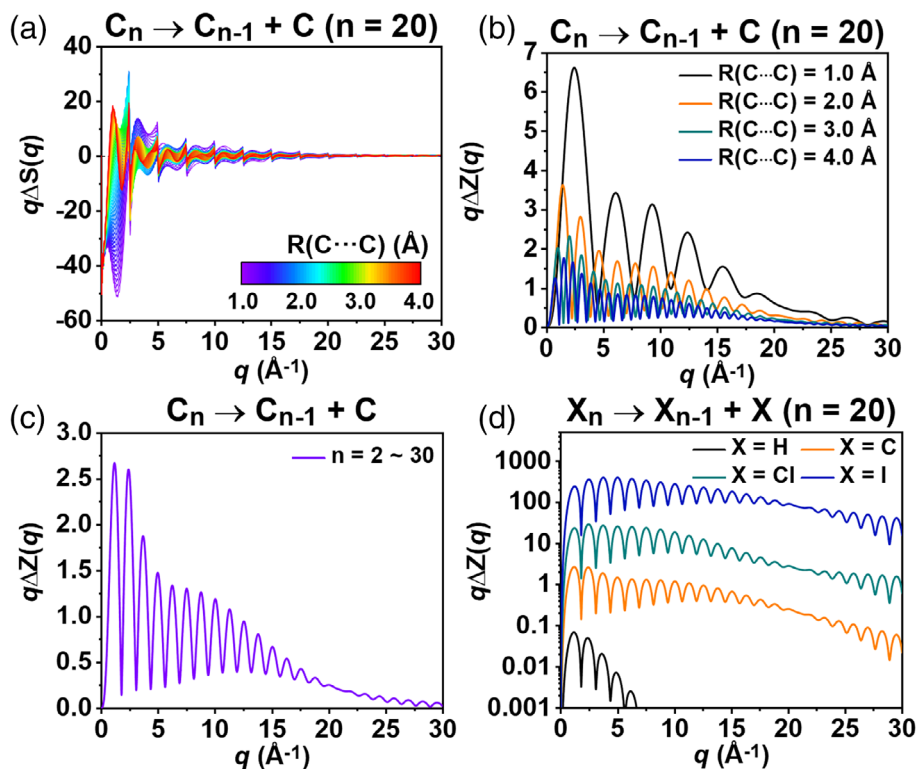


**FIGURE 2** (a)  $q\Delta S(q)$  for  $C_n \rightarrow C_{n-1} + C$ , with  $n = 20$ , calculated for  $R(C\cdots C)$  from 1.0 Å to 4.0 Å of the dissociating  $C\cdots C$  pair in  $C_n$ ,  $R(C-C)$  of nearest  $C-C$  pairs in  $C_n$  and in  $C_{n-1}$  except for  $C\cdots C$  is fixed at 2.5 Å. (b)  $q\Delta Z(q)$  for  $R(C\cdots C)$  in  $C_n$  for the reaction  $C_n \rightarrow C_{n-1} + C$ , for  $n = 20$ .  $q\Delta Z(q)$  is calculated for four different  $R(C\cdots C)$ 's, 1.0, 2.0, 3.0, and 4.0 Å, with  $\Delta r = 0.1$  Å.  $R(C-C)$  is fixed at 2.5 Å as in the case of (a). (c)  $q\Delta Z(q)$  for  $R(C\cdots C)$  in  $C_n$  for the reaction  $C_n \rightarrow C_{n-1} + C$ , for  $n = 2-30$ .  $q\Delta Z(q)$  is calculated for  $R(C\cdots C) = 2.5$  Å with  $\Delta r = 0.1$  Å.  $R(C-C)$  is fixed at 2.5 Å. The resulting  $q\Delta Z(q)$ 's are identical for  $n = 2-30$ , showing that  $q\Delta Z(q)$  does not depend on the size of the molecule. (d)  $q\Delta Z(q)$  for  $R(X\cdots X)$  of the dissociating  $X\cdots X$  pair in  $X_n$  for the reaction  $X_n \rightarrow X_{n-1} + X$  ( $X = H, C, Cl, \text{ and } I$ ), with  $n = 20$ .  $q\Delta Z(q)$  is calculated for  $R(X\cdots X) = 2.5$  Å with  $\Delta r = 0.1$  Å.  $R(X-X)$  is fixed at 2.5 Å

following section. Nevertheless, we note that  $q\Delta Z(q)$  is certainly useful for visualizing the sensitivity of the signal to a structural parameter of interest, as a function of  $q$  as exemplified in Figures 1 and 2.

## Sensitivity of $q\Delta S(q)$ to the changes of atomic positions and structural parameters

### The concept of the sensitivity plot

The TRXL signal sensitively changes in response to the structural changes associated with a reaction. All atoms in the reactant and product molecules contribute to the TRXL signal with a different degree depending on its x-ray scattering factor, and as a result, the sensitivity of the internuclear distance to the TRXL signal varies depending on the corresponding atoms. To quantitatively visualize the sensitivity of atomic positions and internuclear distances to the TRXL signal, we first checked how the atomic position and the internuclear distances quantitatively affect the TRXL signal. Then, we plotted the results in the form of a sensitivity plot on the drawing of the molecular structures of reactant and product molecules. In the sensitivity plot, the sensitivity of the atomic

position is visually indicated with the size of the radius of the atom and that of the internuclear distance with the color of the line representing the internuclear distance.

This concept of the sensitivity plot was introduced in a recent publication.<sup>4</sup> In this scheme, the difference scattering curve ( $\Delta S_{\text{ref}}(q)$ ) arising from a reaction of interest (e.g., the change from a reactant to a product) is calculated and used as a reference. Then, the degree of change in the difference scattering curve with reference to ( $\Delta S_{\text{ref}}(q)$ ) upon the modification of the atomic position or internuclear distance of the participating molecules (e.g., a reactant and a product) is evaluated. The evaluated quantities for various atomic positions or internuclear distances are then averaged and used to draw a sensitivity plot. Here, instead of this scheme, we propose that the concept of  $q\Delta Z(q)$  can be used to draw a sensitivity plot, as explained in the following.

### Sensitivities of $q\Delta S(q)$ to internuclear distances

To quantify the sensitivity of an internuclear distance, we modified the structure by changing the internuclear distance by  $\Delta r$  from the equilibrium distance, while the other internuclear distances are fixed to the reference

distances, as shown in Figure 2 for the calculation of  $q\Delta Z(q)$  for the reaction of a multiatomic molecule. To quantify the dissimilarity between the reference difference scattering curve and the difference scattering curve calculated from the modified structure, of which an internuclear distance is changed, we can calculate  $q\Delta Z(q)$  and use it to quantify the relative sensitivity (RS) of the target internuclear distance. In this way,  $q\Delta Z(q)$  is calculated for all relevant internuclear distances. Here, we set  $\Delta r$ , the structural variance of the internuclear distance, to be 0.1 Å.

In most cases, we are interested in the sensitivity at the overall  $q$  range instead of a specific  $q$ . In this case,  $q\Delta Z(q)$  can be summed up for all  $q$  values. Then  $\sum(q\Delta Z(q))$  values are scaled to yield the RSs by setting the maximum sensitivity for the internuclear distance to be unity. The RSs of the internuclear distances are shown by the color gradient of lines, where the darker color represents the higher RS of the internuclear distance. For example, using this scheme, the RSs of the internuclear distances were calculated for the reaction of  $X-X \rightarrow X-X$ . Figure 3 shows the sensitivity plot drawn based on this scheme. The RS is visualized by the color used to indicate the corresponding internuclear distance. The darker color is used for the larger RS. If RSs at a specific  $q$  need to be

visualized, then  $q\Delta Z(q)$  at the specific  $q$  instead of  $\sum(q\Delta Z(q))$  can be used to calculate RSs.

### Sensitivities of $q\Delta S(q)$ to atomic positions

The sensitivity to the atomic position is evaluated in a similar way to that used for evaluating the sensitivity to the internuclear distance. Each atom in the molecules involved in the reaction of interest is shifted from its reference position, and  $q\Delta Z(q)$  is calculated to quantify the dissimilarity between the reference difference scattering curve and the difference scattering curve calculated from the modified structure, in which an atom is translated by  $r_j$ . For shifting the atomic position, we used the evenly spaced coordinates generated by the spiral method described in the previous work. Specifically, we generated 300 different structures with varying the position of the atom. For each structure, the position of the atom in the structure is translated by  $r_j(\Delta r, \theta_j, \varphi_j)$ , which is the coordinate of the  $j$ th point sampled on the surface of a sphere with radius  $\Delta r$  by using the spiral method. The coordinate of the  $j$ th point sampled by using the spiral method is given by the following equation:

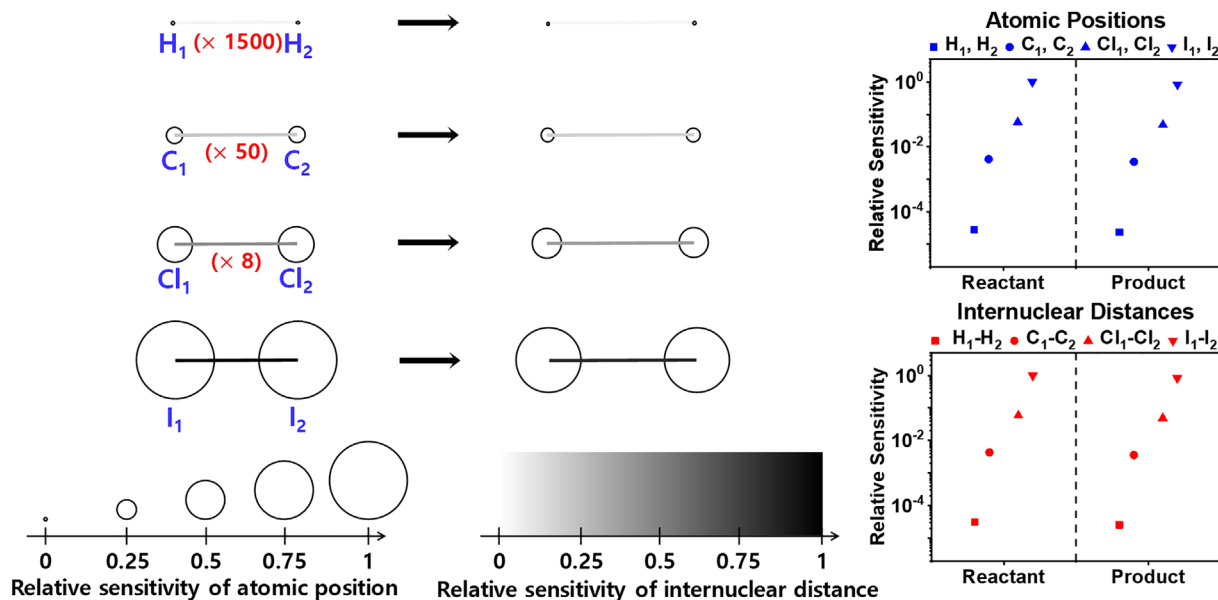


**FIGURE 3** Sensitivity plots for the reaction of  $X-X \rightarrow X-X$  in the gas phase for various types of atoms ( $X = \text{H}, \text{C}, \text{Cl}$ , and  $\text{I}$ ). In the sensitivity plots, the larger radius represents the higher sensitivity of the atomic position, and the darker color represents the higher sensitivity of the internuclear distance. The sensitivity was evaluated by the degree of change of the difference x-ray scattering curve upon altering each atomic position or internuclear distance. To quantitatively estimate the sensitivity, first,  $q\Delta Z(q)$ 's are calculated for the atomic positions and internuclear distances of the reactant,  $X-X$ , and product,  $X-X$ . Then,  $q\Delta Z(q)$ 's are summed up for all  $q$  values to yield  $\sum(q\Delta Z(q))$ . The  $\sum(q\Delta Z(q))$  values were scaled to yield the relative sensitivity (RS) by setting the maximum sensitivity for the atomic position or internuclear distance to be unity. Here, the  $\sum(q\Delta Z(q))$  values for the position of the iodine atoms or the internuclear distance of  $\text{R}(\text{I}-\text{I})$  are the maxima, and thus the sensitivities for the cases of other atoms are scaled with respect to those of the  $\text{I}_2$  case. The RSs are calculated for the molecular structures of the reactant and product with  $\text{R}(\text{X}-\text{X}) = 2.5$  Å and  $\text{R}(\text{X}-\text{X}) = 3.0$  Å. The shift of atomic positions or internuclear distances with an amplitude of 0.1 Å, that is,  $\Delta r = 0.1$  Å, is used to calculate RSs. The numbers in parentheses indicate the multiplication factors, without which the circles to represent the RSs are too small to be visible due to their low sensitivities. Because those for  $\text{H}_2$ ,  $\text{C}_2$ , and  $\text{Cl}_2$  are too small, their RSs are multiplied by the factors shown in the figure. Internuclear distances with RSs below a certain threshold are not shown for simplicity. The scatter plots represent the RSs of the atomic positions and internuclear distances

$$\theta_j = \arccos\left(\frac{2j-1-J}{J}\right) \quad (5)$$

$$\varphi_j = \sqrt{\pi J} \arcsin\left(\frac{2j-1-J}{J}\right) \quad (6)$$

where  $J$  is the total number of the coordinates on the spiral of the sphere and  $j = 1, 2, \dots, J$ . Here,  $\Delta r$ , the structural variance of the atomic position, of 0.1 Å and  $J$  of 300 were used for this simulation.  $q\Delta S_i(q)$ s are calculated using 300 structures generated by the spiral method, and  $q\Delta Z(q)$  is calculated using  $q\Delta S_i(q)$ s. As in the case of the internuclear distances,  $q\Delta Z(q)$  or  $\sum(q\Delta Z(q))$  values are scaled to yield the RSs by setting the maximum sensitivity for the atomic position to be unity. By setting the maximum sensitivity for the atomic position to be unity, the sensitivities to the atomic positions are scaled to yield the RSs. Figure 3 shows the sensitivity plots drawn based on this scheme for the reaction of  $X-X \rightarrow X-X$ . The RS is visualized by the radii of circles representing the atoms. In other words, the larger radius represents the higher sensitivity of the atomic position. The whole  $q$  range of 0–30 Å<sup>-1</sup> is used for Figure 3. To check the dependence of the sensitivity plots on  $q$ , we also draw the sensitivity plots at three  $q$  values of 0.5, 7.0, and 30 Å<sup>-1</sup> in Figure 4a–c.

The plots reveal that the sensitivities depend significantly on the  $q$  value as well as the constituting atoms. The relative importance of heavier and lighter atoms is higher at the larger and smaller  $q$ , respectively. The  $q$ -dependent  $q\Delta Z(q)$  and summed  $q\Delta Z(q)$  can offer different and complementary information on the sensitivity. The  $q$ -dependent  $q\Delta Z(q)$  would be useful for determining the  $q$  range that should be included for the analysis for a specific purpose. For example, it can be inferred that the low  $q$  region should be included for the analysis of H<sub>2</sub> to increase the sensitivity since the RS of the H atom is larger in the low  $q$  region, as shown in Figure 4. On the other hand, the summed  $q\Delta Z(q)$  quantitatively shows to which structural parameters the TRXL signal measured for a given  $q$  range is sensitive. In other words, the summed  $q\Delta Z(q)$  shows which structural parameters among numerous structural parameters of a molecule can be reliably retrieved from the TRXL signal measured for the given  $q$  range (Figure 3).

### Sensitivity plots for the solution phase

Now, we consider how  $q\Delta Z(q)$  behaves for the TRXL data, which contain the cage term and solvent heating term as well as the solute-only term, which corresponds to the gas-phase signal. First, we consider the simplest case

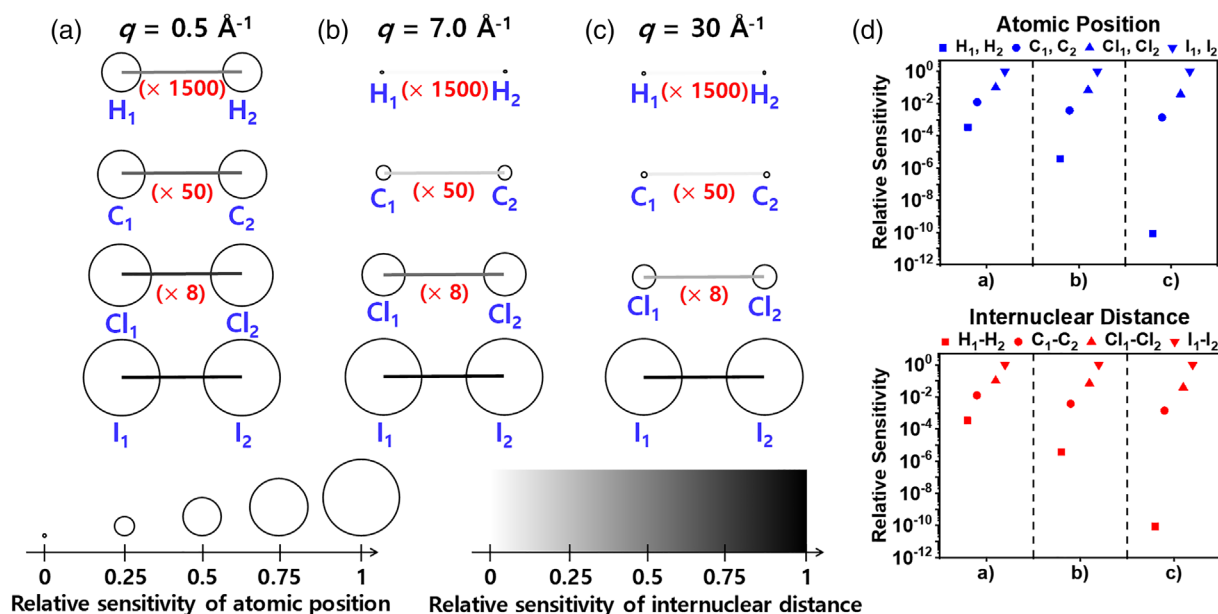


**FIGURE 4** Sensitivity plots for the reaction of  $X-X \rightarrow X-X$  in the gas phase ( $X = \text{H, C, Cl, and I}$ ), at three  $q$  values of (a) 0.5 Å<sup>-1</sup>, (b) 7.0 Å<sup>-1</sup>, and (c) 30 Å<sup>-1</sup>. The relative sensitivities (RSs) are calculated for the molecular structures of the reactant and product with  $R(X-X) = 2.5$  Å and  $R(X-X) = 3.0$  Å.  $\Delta r = 0.1$  Å is used for the calculation of relative sensitivities both for the atomic position and internuclear distance. For the sake of simplicity, only the reactants are displayed by omitting the products. For each case of  $q$ , the maximum RS, which is with the I atoms and the I-I internuclear distances, is set to be unity. The numbers in parentheses indicate the multiplication factors, without which the circles to represent the RSs are too small to be visible due to their low sensitivities. The plots reveal that the RSs depend significantly on the  $q$  value as well as the constituting atoms. Please note that the RSs are calculated just at the  $q$  value specified on the top of the figure, not for a range of  $q$ . For example, the RSs plotted in Figure 4c are calculated just at the  $q$  value of  $q = 30$  Å<sup>-1</sup>, not at the range of  $q$  values of  $q = 0-30$  Å<sup>-1</sup>.

considered in the previous section,  $X_2 \rightarrow X + X$ , in various solvents (methanol, cyclohexane, water, and acetonitrile). As explained earlier, MD simulations are needed to calculate the cage term. Here, since the accuracy of the cage term is not important, we used an approximate method developed to calculate the cage term conveniently. This method is based on approximating the atoms as hard spheres. In this way,  $g(r)$  can be expressed in a simplified mathematical form without MD simulations. The solvent-only term was generated using Equation (2). The two basis differentials,  $(\partial S/\partial T)_p$  and  $(\partial S/\partial \rho)_T$ , are well known for common solvents.<sup>93</sup>  $\Delta T$  and  $\Delta \rho$  were estimated using the approximate method employed in *S-cube*.<sup>91</sup> Here, we note that the quantitative determination of the degree of sensitivity of the cage term and the solvent term is not as straightforward as of the solute-only term. This is because the two terms, cage term and solvent term, cannot be directly expressed as a function of the molecular structure of solute, in contrast to the solute-only term, which is simply expressed as a well-known Debye function. Nevertheless, to evaluate the RS of the solvent term and the cage term with respect to the solute-only term, we introduced an indirect method, where the RSs of the cage and solvent terms are estimated from their relative signal amplitudes with respect to that of the solute-only term. More specifically, the RSs of the cage term and solvent term were estimated as follows. First, to estimate a general relationship between the signal amplitude of each of the three terms (solute-only term, cage term, and solvent term) and sensitivity, we examined how the signal amplitude of the solute term is related to the sensitivity. For that purpose, we prepared five pseudo reactions and calculated the difference scattering curve and sensitivity for each pseudo reaction. For the pseudo reactions, we considered replica reactions where all the elements in the reactants and products are replaced with different elements. For a reaction  $\text{HgI}_2 \rightarrow \text{HgI} + \text{I}$  as an example,<sup>59</sup> we calculated the difference scattering curves for each of the following reaction: (1)  $\text{H}-\text{H}-\text{H} \rightarrow \text{H}-\text{H} + \text{H}$ , (2)  $\text{C}-\text{C}-\text{C} \rightarrow \text{C}-\text{C} + \text{C}$ , (3)  $\text{Cl}-\text{Cl}-\text{Cl} \rightarrow \text{Cl}-\text{Cl} + \text{Cl}$ , (4)  $\text{Br}-\text{Br}-\text{Br} \rightarrow \text{Br}-\text{Br} + \text{Br}$ , (5)  $\text{I}-\text{I}-\text{I} \rightarrow \text{I}-\text{I} + \text{I}$ . After that, by inspecting how the amplitude of the signal, especially that of the solute term, is related to the sensitivity for each pseudo reaction, we generated an equation to calculate the sensitivity from the signal amplitude. We calculated the area under the curves (AUC) of those five difference scattering curves using the following equation:

$$\text{AUC} = \int |q \Delta S(q)| dq \quad (7)$$

When we plotted the calculated AUC versus sensitivity, the plot showed that there is a strong positive correlation between the AUC and the sensitivity (data not shown). In fact, we found that the sensitivity can be nicely described using the AUC using the following equation:

$$\log_{10}(\text{sensitivity}) = a(\log_{10}(\text{AUC}))^2 + b(\log_{10}(\text{AUC})) + c \quad (8)$$

Using the five AUCs and sensitivities for the five pseudo reactions, we optimized the parameters  $a$ ,  $b$ , and  $c$ . Then, we used Equation (8) with the determined parameters to estimate the sensitivities of the cage and solvent terms of the target reaction, for example,  $\text{HgI}_2 \rightarrow \text{HgI} + \text{I}$  in this case. The AUC of the cage and solvent terms of the target reaction were calculated using *S-cube*. Finally, from the AUCs of these terms, we estimated the sensitivities of the cage term and the solvent term based on Equation (8), and RSs were calculated using the sensitivity values by normalization of the values with respect to the highest sensitivity value of the reaction. It should be noted that the parameters in Equation (8) need to be determined for each target reaction, following the approach described here.

Figure 5a shows the sensitivity plots of  $X_2 \rightarrow X + X$  for the solution phase. Two solvent molecules are indicated as circles to represent the RSs of the cage term and the solvent-only term, respectively. Figure 5b,c shows the sensitivity plots of  $X-X \rightarrow X-X$  and  $X_n \rightarrow X_{n-1} + X$  ( $X = \text{H}, \text{C}, \text{Cl}$ , and  $\text{I}$ ), with  $n = 20$ , respectively, for the solution phase. In all three reactions, the contributions from the cage and solvent-only terms are comparable to the solute-only term only for the case of  $X = \text{I}$ . In the cases of other atoms ( $X = \text{Cl}, \text{F}$ , and  $\text{H}$ ), the solute-only and cage terms become negligible, and only the solvent-only term is significant. The sensitivity plots of the reactant for  $X_2 \rightarrow X + X$  and  $X-X \rightarrow X-X$  are quite similar, but the sensitivities of the cage term show a considerable difference. The considerably larger cage sensitivity of  $X_2 \rightarrow X + X$  than that of  $X-X \rightarrow X-X$  is caused because the change of the cage structure is much larger in the former reaction than in the latter case. To also check how the sensitivity plots depend on different solvents, the sensitivity plots for  $X-X \rightarrow X-X$  ( $X = \text{I}$ ) for various solvents (methanol, cyclohexane, water, and acetonitrile) are compared (Figure 6). The RS of the solvent term shows noticeable dependence on solvents. For example, among the four solvents tested here, the cyclohexane case has the largest sensitivity to the solvent term.

Finally, Figure 7 lists sensitivity plots for several representative reactions studied by TRXL. Here, the sensitivities of all reactions are plotted on the common scale so that the sensitivities among different reactions can be easily compared. Also, for the sake of comparison, the concentration of the solute species of all reactions is set to be the same at 10 mM. Since the two I atoms in  $\text{HgI}_2$  and the two Hg-I internuclear distances in  $\text{HgI}_2$  of the reaction of  $\text{HgI}_2 \rightarrow \text{HgI} + \text{I}$  have the largest sensitivities, their sensitivities are set to be unities.<sup>59</sup> In general, the sensitivities of the atomic positions of the light atoms (C, N, and H) are low. For example, the atomic positions of C and N of  $[\text{Au}(\text{CN})_2]^-_3$  ( $S_0$ )  $\rightarrow$   $[\text{Au}(\text{CN})_2]^-_3$  ( $T_1$ ) have small sensitivities of

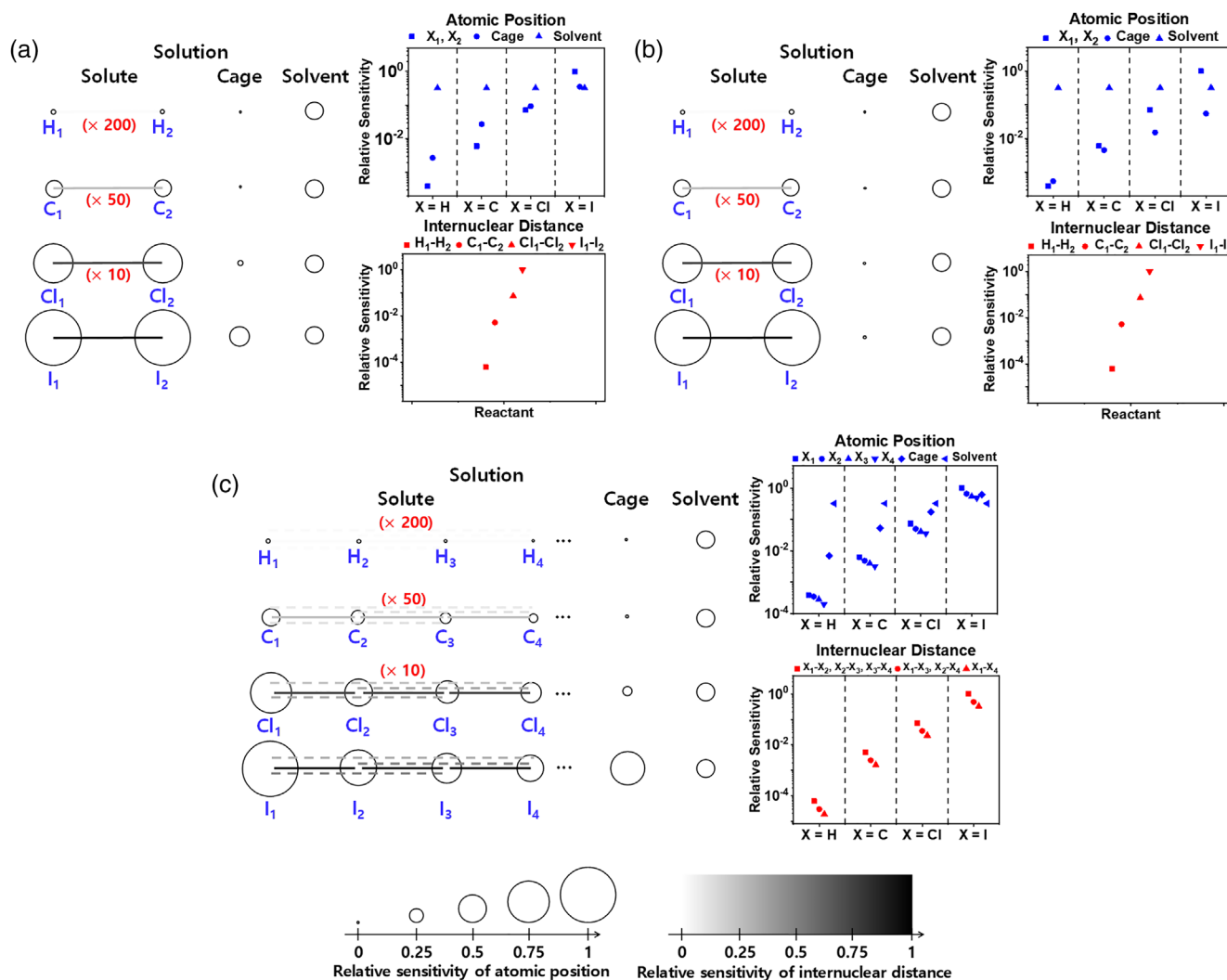


**FIGURE 5** Sensitivity plots for (a)  $X_2 \rightarrow X + X$  and (b)  $X-X \rightarrow X-X$ , and (c)  $X_n \rightarrow X_{n-1} + X$  ( $X = \text{H, C, Cl, and I}$ ), with  $n = 20$ , for the solution phase (in methanol). The relative sensitivities (RSs) are calculated for the molecular structures with (a)  $R(X-X) = 2.5 \text{ \AA}$ , (b)  $R(X-X) = 2.5 \text{ \AA}$  and  $R(X-X) = 3.0 \text{ \AA}$ , and (c)  $R(X-X) = 2.5 \text{ \AA}$  for all nearest  $X-X$  pairs.  $\Delta r = 0.1 \text{ \AA}$  is used for the calculation of RSs both for the atomic position and internuclear distance. For the sake of simplicity, only the reactants are displayed by omitting the products. For each case, the maximum sensitivity, which is with the positions of I atoms and the I-I internuclear distances, is set to be unity. The numbers in parentheses indicate the multiplication factors, without which the circles to represent the sensitivities are too small to be visible due to their low sensitivities. Internuclear distances between atoms forming bonds are indicated in solid lines, and those without bonds are in broken lines. The scatter plots represent the RSs of the atomic positions and internuclear distances. The  $q$  range of  $1-8 \text{ \AA}^{-1}$  is used for the calculation of sensitivity plots

less than 5% compared to the atomic positions of the Au.<sup>71</sup> A notable point from the inspection of RSs for the various reactions is that the RS for the position of an atom is exceptionally small for the atoms located at the center of a symmetric molecule (e.g., Au<sub>2</sub> of  $[\text{Au}(\text{CN})_2]_3$  ( $T_1'$ ) shown in Figure 7f and Fe of  $[\text{Fe}(\text{bpy})_3]^{2+}$  and  $[\text{Fe}(\text{bpy})_3]^{2+*}$  shown in Figure 7g). This insensitivity for the position of an atom, for example, Fe of  $[\text{Fe}(\text{bpy})_3]^{2+}$ , arises because the TRXL signal is indeed insensitive to the position of the atom: in the case when the position of the Fe atom is displaced from the symmetric center of the molecule to elsewhere, the TRXL signal can detect that such a displacement occurred; however, the direction of the displacement of the position of Fe atom cannot be

discriminated from the TRXL signal because, for example, the TRXL signal is the same whether the Fe atom is moved upward, downward, leftward, or rightward.

### Sensitivity plots for determining the optimal $q$ range

As mentioned earlier, the motivation for devising the metric  $q\Delta Z(q)$  is a need for a reasonable, quantitative determination of the optimal experimental condition. The key in determining the optimal experimental conditions is to determine the optimal  $q$  range to be examined. Once the optimal  $q$  range is identified, the experimental

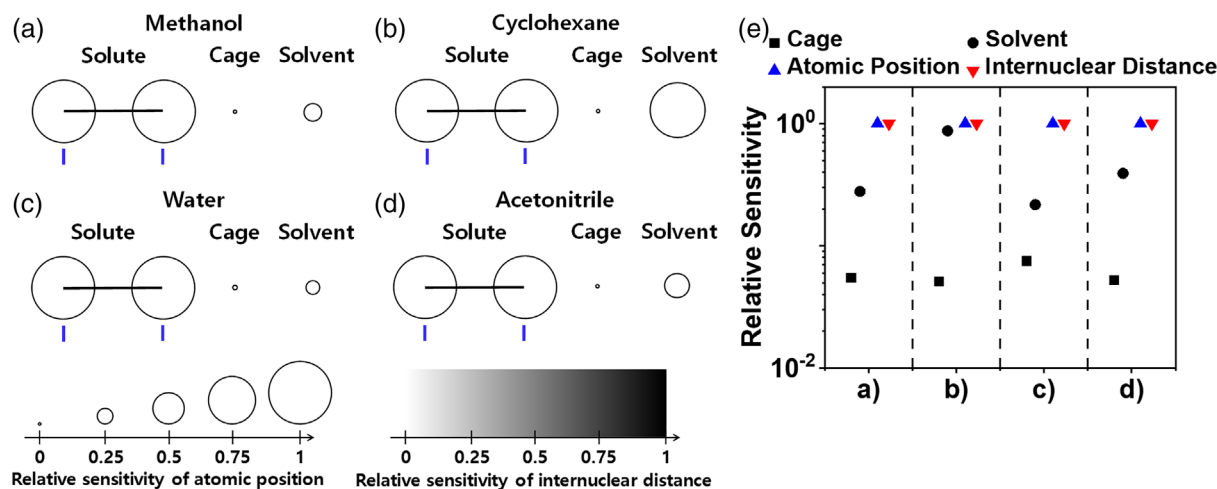


**FIGURE 6** Sensitivity plots for  $X-X \rightarrow X-X$  ( $X = I$ ) for the solution phase with various solvents: (a) methanol, (b) cyclohexane, (c) water, and (d) acetonitrile. The relative sensitivities (RSs) are calculated for the molecular structures with  $R(X-X) = 2.5 \text{ \AA}$  and  $R(X-X) = 3.0 \text{ \AA}$ .  $\Delta r = 0.1 \text{ \AA}$  is used for the calculation of relative sensitivities both for the atomic position and internuclear distance. (e) Scatter plots of the RSs of the atomic position and internuclear distance. For the sake of simplicity, only the reactants are displayed by omitting the products. For each case, the maximum sensitivity, which is with the positions of I atoms and the I-I internuclear distances, is set to be unity. The  $q$  range of  $1-8 \text{ \AA}^{-1}$  is used for the calculation of sensitivity plots

parameters such as sample-to-detector distance and x-ray photon energy can be optimized according to the predetermined  $q$  region and the size of the available detector. For the ideal case where one can obtain clean data free from any experimental noise, a  $q$  range as wide as possible would be better. This is because the data in a wider  $q$  range provide richer structural information and thus would result in a better structural resolution. In reality, the experimental data contain noise, and the higher the  $q$ , the larger the noise level and the weaker the signal strength. Therefore, it is inevitable to compromise the  $q$  range in order to conduct the experiment efficiently within limited beamtime: it is required to cover a  $q$  range as wide as possible within the region where the signal is not overwhelmed by noise.

For that purpose, here we propose a criterion for determining the optimal  $q$  range based on  $q\Delta Z(q)$ : the optimal  $q$  range is the region where  $\Delta Z(q)$ , which is  $q\Delta Z(q)$  divided by  $q$ , is larger than the expected noise level of the experiment ( $\sigma_{\text{exp}}(q)$ ). In other words, the optimal  $q$  range is the region where  $q\Delta Z(q)$  is larger than  $\sigma_{\text{exp}}(q)$  multiplied by  $q$  (that is,  $q\sigma_{\text{exp}}(q)$ ). This criterion is devised based on the traditional method of determining whether the experiment is feasible by comparing the noise and signal levels expected for the experiment.<sup>91</sup> Such a traditional criterion assumes that data measured at a  $q$  point would be meaningful only when the signal amplitude is larger than the amplitude of the noise. Likewise, the criteria we propose here are based on the following assumption: a signal measured at a  $q$  point is meaningful only when the degree to which the signals of the different structures differ (i.e., represented quantitatively by the measure,  $q\Delta Z(q)$ ) is large enough to overcome the noise level of the experiment. This assumption also

means that  $\Delta Z(q)$  sets the upper limit of the experimental noise level,  $\sigma_{\text{exp}}(q)$ , necessary for detecting the target structural change. It should be noted that the amplitude of  $q\Delta Z(q)$  is dependent on the structural variance,  $\Delta r$ , of the structural parameter. We suggest that if there is a desired level of structural resolution, for example,  $x \text{ \AA}$  resolution of a specific structural parameter, to be achieved for the experiment, the optimal  $q$  range can be calculated by taking into account the desired level of the structural resolution. More specifically, by comparing  $q\sigma_{\text{exp}}(q)$  with  $q\Delta Z(q)$  calculated under the degree of structural variance  $\Delta r = x \text{ \AA}$ , one can determine (1) whether it is feasible to retrieve the structural parameter from the experiment with the desired level of the structural resolution, and (2) what is the optimal  $q$  range for the experiment.

Based on the criteria, here we demonstrate an example showing how the optimal  $q$  range can be determined. In Figure 8, we compared  $q\Delta Z(q)$  of the reactions  $X_2 \rightarrow X + X$  ( $X = H, C, Cl, \text{ and } I$ ) in the solution phase with  $q\sigma_{\text{exp}}(q)$ . For the estimation of  $q\Delta Z(q)$  and  $q\sigma_{\text{exp}}(q)$ , we assumed that 10 mM of  $X_2$  with  $R(X-X)$  of  $2.5 \text{ \AA}$  dissolved in cyclohexane is converted to yield 20 mM of product,  $X$ , and the data are collected at the ID09 beamline of ESRF. Then,  $q\Delta Z(q)$  was calculated assuming the structural variance ( $\Delta r$ ) of  $R(X-X)$  of  $0.1 \text{ \AA}$ . Following the criteria, the optimal  $q$  region can be determined to be the region where  $q\Delta Z(q)$  is higher than  $q\sigma_{\text{exp}}(q)$ . Here, it should be noted that  $q\sigma_{\text{exp}}(q)$  is dependent on the experimental parameters, especially on the data accumulation time, because the signal-to-noise ratio (SNR) of the data is dependent on the number of scattering images collected per a time delay.<sup>91</sup> Accordingly, the optimal  $q$  range of the experiment is dependent on the accumulation time.



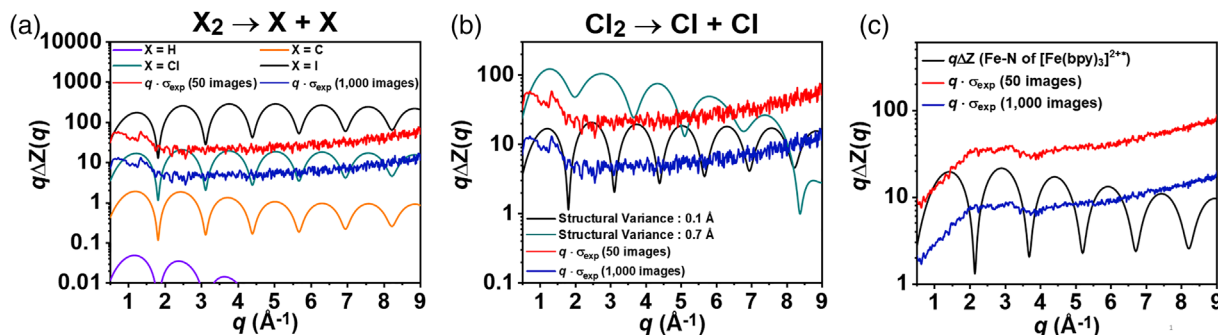


**FIGURE 8** (a) Comparison of  $q\Delta Z(q)$  and  $q\sigma_{\text{exp}}(q)$  for the reactions  $X_2 \rightarrow X + X$  ( $X = \text{I, Cl, C, H}$ ) in solution.  $q\Delta Z(q)$  is calculated for  $R(X-X)$  with  $\Delta r = 0.1 \text{ \AA}$ .  $q\sigma_{\text{exp}}(q)$  is estimated assuming 50 and 1000 difference scattering images are accumulated for each data with 1.5 s exposure time for each image. It is assumed that 10 mM of  $X_2$  dissolved in cyclohexane undergoes the reaction to yield  $2X$  and  $R(X-X)$  is  $2.5 \text{ \AA}$ . (b) Comparison of  $q\Delta Z(q)$  and  $q\sigma_{\text{exp}}(q)$  for the reaction  $\text{Cl}_2 \rightarrow \text{Cl} + \text{Cl}$  in solution. Here,  $q\Delta Z(q)$  is calculated under two different degrees of structural variances of  $R(\text{Cl}-\text{Cl})$ ,  $\Delta r = 0.1 \text{ \AA}$  and  $\Delta r = 0.7 \text{ \AA}$ . The other conditions are the same as those for (a). (c) Comparison of  $q\Delta Z(q)$  and  $q\sigma_{\text{exp}}(q)$  for the reaction  $[\text{Fe}(\text{bpy})_3]^{2+} \rightarrow [\text{Fe}(\text{bpy})_3]^{2+*}$ . The superscript \* indicates an electronic excited state. For the reaction, it is assumed that the electronic transition accompanies Fe–N bond elongation from about  $1.96 \text{ \AA}$  to  $2.10 \text{ \AA}$ .  $q\Delta Z(q)$  (black solid line) is calculated for  $R(\text{Fe}-\text{N})$  of  $[\text{Fe}(\text{bpy})_3]^{2+*}$  with  $0.1 \text{ \AA}$  structural variance.  $q\sigma_{\text{exp}}(q)$  is estimated assuming that 50 mM of  $[\text{Fe}(\text{bpy})_3]^{2+}$  dissolved in water undergoes the structural change.  $q\sigma_{\text{exp}}(q)$  for 50 (red solid line) and 1000 (blue solid line) accumulated images are estimated assuming that exposure time for each difference scattering is 1.5 s

dependent on the degree of structural variance of the structural parameter, we calculated the  $q\Delta Z(q)$  with varying the structural variance.

As shown in Figure 8a, when a small number (50) of images are collected per a time delay,  $q\sigma_{\text{exp}}(q)$  is always higher than  $q\Delta Z(q)$  of the reactions  $X_2 \rightarrow X + X$  except for the case of  $X = \text{I}$ . This comparison directly shows that 50 images per time delay is not enough to resolve the structural change of  $\text{Cl}_2$ ,  $\text{C}_2$ , or  $\text{H}_2$ . For the reaction  $\text{I}_2 \rightarrow \text{I} + \text{I}$ ,  $q\Delta Z(q)$  is higher than  $q\sigma_{\text{exp}}(q)$  throughout the examined region ( $q = 0.5\text{--}9 \text{ \AA}^{-1}$ ), indicating that all the examined regions fall within the optimal  $q$  range. When a larger number (1000) of images are collected per time delay, the signal from the reaction  $\text{Cl}_2 \rightarrow \text{Cl} + \text{Cl}$  also can be obtained with a quality sufficient to resolve the structural change of  $\text{Cl}_2$ . For the experiment, the optimal  $q$  range would be about  $q < 8.9 \text{ \AA}^{-1}$ . Still, the quality of the signal is insufficient for the reactions  $\text{C}_2 \rightarrow \text{C} + \text{C}$  and reactions  $\text{H}_2 \rightarrow \text{H} + \text{H}$ . Figure 8b shows how the optimal  $q$  range changes depending on the desired level of the precision of the structural analysis. For the reaction  $\text{Cl}_2 \rightarrow \text{Cl} + \text{Cl}$ , if the goal of the experiment is to retrieve the Cl–Cl distance

with an accuracy of about  $0.1 \text{ \AA}$  (the corresponding  $q\Delta Z(q)$  is shown in a blue solid line), the data obtained by accumulating 50 difference scattering images would not be of quality high enough to achieve the desired structural resolution because the large experimental noise ( $q\sigma_{\text{exp}}(q)$ , represented by red solid line) would make it impossible to discern the difference in the experimental signal due to the structural change of the order of  $0.1 \text{ \AA}$  (blue solid line). To distinguish the desired difference in the TRXL signal, one needs to accumulate as many images as 1000. However, if the goal of the experiment is rather to roughly estimate the structural parameter, for example, the Cl–Cl distance with an accuracy of  $0.7 \text{ \AA}$  (the corresponding  $q\Delta Z(q)$  is shown in a turquoise solid line), such a goal can be achieved with the data obtained by accumulating only 50 difference scattering images. The optimal  $q$  range is also highly dependent on the desired level of structural precision. When the goal of the experiment is a rough estimate of the molecular structure (turquoise solid line in Figure 8b), the  $q\Delta Z(q)$  significantly diminishes at the high- $q$  region ( $q > 7 \text{ \AA}^{-1}$ ), indicating that it is less desirable to cover the high- $q$  region. However,

**FIGURE 7** Sensitivity plots for various representative reactions studied with TRXL. (a)  $\text{HgI}_2 \rightarrow \text{HgI} + \text{I}$  in methanol.<sup>59</sup> (b)  $\text{HgBr}_2 \rightarrow \text{HgBr} + \text{Br}$  in methanol.<sup>23,59</sup> (c)  $\text{CH}_2\text{I}_2 \rightarrow \text{CH}_2\text{I} + \text{I}$  in methanol.<sup>60,75</sup> (d)  $\text{C}_2\text{H}_4\text{I}_2 \rightarrow \text{bridged-}\text{C}_2\text{H}_4\text{I} + \text{I}$  in cyclohexane.<sup>7,33</sup> (e)  $\text{C}_2\text{F}_4\text{I}_2 \rightarrow \text{anti-}\text{C}_2\text{F}_4\text{I} + \text{I}$  in cyclohexane.<sup>94</sup> (f)  $[\text{Au}(\text{CN})_2]_3 (\text{S}_0) \rightarrow [\text{Au}(\text{CN})_2]_3 (\text{T}_1)$  in water.<sup>71</sup> (g)  $[\text{Fe}(\text{bpy})_3]^{2+} (R(\text{Fe}-\text{N}) = 1.96 \text{ \AA}) \rightarrow [\text{Fe}(\text{bpy})_3]^{2+*} (R(\text{Fe}-\text{N}) = 2.10 \text{ \AA})$  in water.<sup>95</sup> Here, the sensitivities of all reactions are plotted on the common scale so that the sensitivities among different reactions can be easily compared.  $\Delta r = 0.1 \text{ \AA}$  is used for the calculation of relative sensitivities for both the atomic position and internuclear distance. Since the positions of two I atoms in  $\text{HgI}_2$  and the two Hg–I internuclear distances in  $\text{HgI}_2$  of the reaction of  $\text{HgI}_2 \rightarrow \text{HgI} + \text{I}$  in (a) have the largest sensitivities among all reactions considered here, their sensitivities are set to be unities. Internuclear distances between atoms forming bonds are indicated in solid lines, and those without bonds are in broken lines. Internuclear distances with sensitivities below a certain threshold are omitted for simplicity. We note that the sensitivity is dependent on the concentration of the solutes participating in the reaction. For the sake of comparison, the concentration of the solute species of all reactions is set to be the same at 10 mM. The 1D scatter plots represent the relative sensitivities (RSs) of the atomic position and internuclear distance with a log scale. The  $q$  range of  $1\text{--}8 \text{ \AA}^{-1}$  is used for the calculation of sensitivity plots. Since all the atoms corresponding to each element showed similar values of RS in (g), the average value of the RSs for each element is expressed as a point in the scatter plot, and the standard deviation of the RSs for each element is expressed as an error bar

when determining the molecular structure with a higher precision (black solid line in Figure 8b), the  $q\Delta Z(q)$  of the high- $q$  region becomes similar or even larger than that of the low- $q$  region, implying that it is desirable to cover the high- $q$  region.

The criterion for determining the optimal  $q$  range, which we propose in this work, is applicable not only to the reaction of simple molecules, such as  $X_2 \rightarrow X + X$  shown in Figure 8a,b, but also to the reaction of complicated molecules, such as organometallic complexes. Here, we also show an example with more complex molecular geometry, namely,  $[\text{Fe}(\text{bpy})_3]^{2+}$  dissolved in water (See Figure 8c). For this molecule, we estimated  $q\Delta Z(q)$  and  $q\sigma_{\text{exp}}(q)$  assuming that 50 mM of  $[\text{Fe}(\text{bpy})_3]^{2+}$  dissolved in water is photoexcited to its high spin state and the data are collected at the ID09 beamline of ESRF with the exposure time per image of 1.5 s. We assume that the spin-state transition accompanies Fe–N bond elongation from about 1.9 Å to 2.1 Å.<sup>95</sup> The result shows that to resolve the Fe–N distance in the short-lived excited state with about 0.1 Å resolution, one needs to obtain a large number, about 1000, of images. And in that case, the optimal  $q$  range would be from  $q = 0.5 \text{ \AA}^{-1}$  or smaller to about  $q = 6.2 \text{ \AA}^{-1}$ .

## CONCLUSION

### Summary and outlook

In this work, we introduced a systematic method to quantify and visualize the sensitivities of the atomic positions and the internuclear distances to the TRXL signal, even as a function of  $q$  if desired. The devised sensitivity plots should facilitate easy estimation of the relative contributions of three components constituting the TRXL signal (the solute-only term, the cage term, and the solvent-only term), thereby making it possible to examine whether the expected TRXL signal from a target molecular system is sensitive enough to the atomic positions and internuclear distances of interest compared to other atomic positions and internuclear distances. In addition, the sensitivity plots as a function of  $q$  should aid in determining the optimal  $q$  range, x-ray energy and sample-to-detector distance for the experiment so that the beamtime, which is generally highly competitive, can be used to produce the maximum output.

The consideration of  $q\Delta Z(q)$  confirms that for a certain target reaction, the maximum  $q$  of the optimal  $q$  range exceeds  $9 \text{ \AA}^{-1}$ , depending on the experimental parameters such as the exposure time and the number of accumulations per time delay. In this regard, it is notable that recently, x-ray facilities such as the european synchrotron radiation facility (ESRF) or the linac coherent light source (LCLS) are providing, or planning to provide, high-energy

x-rays up to  $\sim 25 \text{ keV}$ , which can extend the accessible  $q$  range of the TRXL experiments to an unprecedented level, for example, up to  $15 \text{ \AA}^{-1}$ . Definitely, accessibility to such a high- $q$  range would provide a new opportunity to the users of the TRXL experiment. Nevertheless, the use of such a high-energy x-ray is not always beneficial: it depends on the goal of the experiment and the reaction. Accordingly, it will be crucial to decide which x-ray energy, for example, 25 keV or 12 keV, is optimal for the goal of the experiment, and our proposed  $q\Delta Z(q)$  metric should aid in determining the optimal x-ray energy.

We note that in principle, the proposed method should be applicable to not only TRXL but also other scattering methods such as ultrafast electron diffraction<sup>94,96–98</sup> and femtosecond x-ray scattering in the gas phase.

## Distribution

We import and distribute the function to plot the sensitivity presented in this work as a MATLAB app, *S-cube*, which can simulate the TRXL data and has already been distributed by Kim et al.<sup>91</sup> The function of the sensitivity plot presented in this work is imported to version 3.4 or a later version of *S-cube*. The *S-cube* program (doi: 10.5281/zenodo.3637919) is distributed in <https://zenodo.org/badge/latestdoi/207274974> as well as the GitHub repository (<https://github.com/Jkim9486/Scube>).

## ACKNOWLEDGMENTS

This work was supported by the Institute for Basic Science (IBS-R033).

## REFERENCES

- [1] H. Ihee, *Acc. Chem. Res.* **2009**, *42*, 356.
- [2] J. G. Kim, T. W. Kim, J. Kim, H. Ihee, *Acc. Chem. Res.* **2015**, *48*, 2200.
- [3] H. Ki, K. Y. Oang, J. Kim, H. Ihee, *Annu. Rev. Phys. Chem.* **2017**, *68*, 473.
- [4] J. G. Kim, E. H. Choi, Y. Lee, H. Ihee, *Acc. Chem. Res.* **2021**, *54*, 1685.
- [5] R. Neutze, R. Wouts, S. Techert, J. Davidsson, M. Kocsis, A. Kirrander, F. Schotte, N. Wulff, *Phys. Rev. Lett.* **2001**, *87*, 195508.
- [6] H. Ihee, M. Lorenc, T. K. Kim, Q. Y. Kong, M. Cammarata, J. H. Lee, S. Bratos, M. Wulff, *Science* **2005**, *309*, 1223.
- [7] Q. Kong, J. Kim, M. Lorenc, T. K. Kim, H. Ihee, M. Wulff, *J. Phys. Chem. A* **2005**, *109*, 10451.
- [8] A. Plech, V. Kotaidis, M. Lorenc, M. Wulff, *Chem. Phys. Lett.* **2005**, *401*, 565.
- [9] M. Cammarata, M. Lorenc, T. K. Kim, J. H. Lee, Q. Y. Kong, E. Pontecorvo, M. L. Russo, G. Schiró, A. Cupane, M. Wulff, H. Ihee, *J. Chem. Phys.* **2006**, *124*, 124504.
- [10] T. K. Kim, M. Lorenc, J. H. Lee, M. Lo Russo, J. Kim, M. Cammarata, Q. Kong, S. Noel, A. Plech, M. Wulff, H. Ihee, *Proc. Natl. Acad. Sci. U. S. A.* **2006**, *103*, 9410.
- [11] J. H. Lee, K. H. Kim, T. K. Kim, Y. Lee, H. Ihee, *J. Chem. Phys.* **2006**, *125*, 174504.
- [12] M. Wulff, S. Bratos, A. Plech, R. Vuilleumier, F. Mirloup, M. Lorenc, Q. Kong, H. Ihee, *J. Chem. Phys.* **2006**, *124*, 034501.
- [13] Q. Kong, M. Wulff, J. H. Lee, S. Bratos, H. Ihee, *J. Am. Chem. Soc.* **2007**, *129*, 13584.

- [14] J. H. Lee, T. K. Kim, J. Kim, M. Lorenc, Q. Kong, M. Wulff, H. Ihee, *AIP Conf. Proc.* **2007**, 879, 1262.
- [15] M. Wulff, Q. Kong, M. Cammarata, M. L. Russo, P. Anfinrud, F. Schotte, M. Lorenc, H. Ihee, T. K. Kim, A. Plech, *AIP Conf. Proc.* **2007**, 879, 1187.
- [16] M. Cammarata, M. Levantino, F. Schotte, P. A. Anfinrud, F. Ewald, J. Choi, A. Cupane, M. Wulff, H. Ihee, *Nat. Methods* **2008**, 5, 881.
- [17] Q. Kong, J. H. Lee, A. Plech, M. Wulff, H. Ihee, M. H. Koch, *Angew. Chem., Int. Ed.* **2008**, 47, 5550.
- [18] J. H. Lee, J. Kim, M. Cammarata, Q. Kong, K. H. Kim, J. Choi, T. K. Kim, M. Wulff, H. Ihee, *Angew. Chem., Int. Ed.* **2008**, 47, 1047.
- [19] J. H. Lee, T. K. Kim, J. Kim, Q. Kong, M. Cammarata, M. Lorenc, M. Wulff, H. Ihee, *J. Am. Chem. Soc.* **2008**, 130, 5834.
- [20] S. Ahn, K. H. Kim, Y. Kim, J. Kim, H. Ihee, *J. Phys. Chem. B* **2009**, 113, 13131.
- [21] M. Christensen, K. Haldrup, K. Bechgaard, R. Feidenhans'l, Q. Y. Kong, M. Cammarata, M. Lo Russo, M. Wulff, N. Harrit, M. M. Nielsen, *J. Am. Chem. Soc.* **2009**, 131, 502.
- [22] K. Ichiyangi, T. Sato, S. Nozawa, K. H. Kim, J. H. Lee, J. Choi, A. Tomita, H. Ichikawa, S. Adachi, H. Ihee, S. Koshihara, *J. Synchrotron Radiat.* **2009**, 16, 391.
- [23] S. Jun, J. H. Lee, J. Kim, J. Kim, K. H. Kim, Q. Kong, T. K. Kim, M. Lo Russo, M. Wulff, H. Ihee, *Phys. Chem. Chem. Phys.* **2010**, 12, 11536.
- [24] Q. Kong, J. H. Lee, M. Lo Russo, T. K. Kim, M. Lorenc, M. Cammarata, S. Bratos, T. Buslaps, V. Honkimaki, H. Ihee, M. Wulff, *Acta Cryst. A* **2010**, 66, 252.
- [25] Q. Kong, J. H. Lee, K. H. Kim, J. Kim, M. Wulff, H. Ihee, M. H. J. Koch, *J. Am. Chem. Soc.* **2010**, 132, 2600.
- [26] K. Haldrup, T. Harlang, M. Christensen, A. Dohn, T. B. van Driel, K. S. Kjaer, N. Harrit, J. Vibenholt, L. Guerin, M. Wulff, M. M. Nielsen, *Inorg. Chem.* **2011**, 50, 9329.
- [27] S. Ibrahimkutty, J. Kim, M. Cammarata, F. Ewald, J. Choi, H. Ihee, A. Plech, *ACS Nano* **2011**, 5, 3788.
- [28] J. Kim, K. H. Kim, J. G. Kim, T. W. Kim, Y. Kim, H. Ihee, *J. Phys. Chem. Lett.* **2011**, 2, 350.
- [29] K. H. Kim, K. Y. Oang, J. Kim, J. H. Lee, Y. Kim, H. Ihee, *Chem. Commun.* **2011**, 47, 289.
- [30] P. L. Ramachandran, J. E. Lovett, P. J. Carl, M. Cammarata, J. H. Lee, Y. O. Jung, H. Ihee, C. R. Timmel, J. J. van Thor, *J. Am. Chem. Soc.* **2011**, 133, 9395.
- [31] L. Guerin, Q. Kong, D. Khakhulin, M. Cammarata, H. Ihee, M. Wulff, *Synchrotron Radiat. News* **2012**, 25, 25.
- [32] T. W. Kim, J. H. Lee, J. Choi, K. H. Kim, L. J. van Wilderen, L. Guerin, Y. Kim, Y. O. Jung, C. Yang, J. Kim, M. Wulff, J. J. van Thor, H. Ihee, *J. Am. Chem. Soc.* **2012**, 134, 3145.
- [33] J. Kim, J. H. Lee, J. Kim, S. Jun, K. H. Kim, T. W. Kim, M. Wulff, H. Ihee, *J. Phys. Chem. A* **2012**, 116, 2713.
- [34] K. H. Kim, S. Muniyappan, K. Y. Oang, J. G. Kim, S. Nozawa, T. Sato, S.-Y. Koshihara, R. Henning, I. Kosheleva, H. Ki, Y. Kim, T. W. Kim, J. Kim, S.-I. Adachi, H. Ihee, *J. Am. Chem. Soc.* **2012**, 134, 7001.
- [35] K. H. Kim, H. Ki, K. Y. Oang, S. Nozawa, T. Sato, J. Kim, T. K. Kim, J. Kim, S.-I. Adachi, H. Ihee, *ChemPhysChem* **2013**, 14, 3687.
- [36] J. H. Lee, M. Wulff, S. Bratos, J. Petersen, L. Guerin, J.-C. Leicknam, M. Cammarata, Q. Kong, J. Kim, K. B. Møller, H. Ihee, *J. Am. Chem. Soc.* **2013**, 135, 3255.
- [37] T. W. Kim, J. G. Kim, C. Yang, H. Ki, J. Jo, H. Ihee, *Bull. Korean Chem. Soc.* **2014**, 35, 695.
- [38] K. Y. Oang, J. G. Kim, C. Yang, T. W. Kim, Y. Kim, K. H. Kim, J. Kim, H. Ihee, *J. Phys. Chem. Lett.* **2014**, 5, 804.
- [39] K. Y. Oang, K. H. Kim, J. Jo, Y. Kim, J. G. Kim, T. W. Kim, S. Jun, J. Kim, H. Ihee, *Chem. Phys.* **2014**, 422, 137.
- [40] H. Takala, A. Bjorling, O. Berntsson, H. Lehtivuori, S. Niebling, M. Hoernke, I. Kosheleva, R. Henning, A. Menzel, J. A. Ihalainen, S. Westenhoff, *Nature* **2014**, 509, 245.
- [41] K. H. Kim, H. Ki, J. H. Lee, S. Park, Q. Kong, J. Kim, J. Kim, M. Wulff, H. Ihee, *Phys. Chem. Chem. Phys.* **2015**, 17, 8633.
- [42] K. H. Kim, J. Kim, K. Y. Oang, J. H. Lee, D. Grolimund, C. J. Milne, T. J. Penfold, S. L. Johnson, A. Galler, T. W. Kim, J. G. Kim, D. Suh, J. Moon, J. Kim, K. Hong, L. Guérin, T. K. Kim, M. Wulff, C. Bressler, H. Ihee, *Phys. Chem. Chem. Phys.* **2015**, 17, 23298.
- [43] E. Malmerberg, P. H. M. Bovee-Geurts, G. Katona, X. Deupi, D. Arnlund, C. Wickstrand, L. C. Johansson, S. Westenhoff, E. Nazarenko, G. F. X. Schertler, A. Menzel, W. J. de Grip, R. Neutze, *Sci. Signaling* **2015**, 8, 8.
- [44] A. Björling, O. Berntsson, H. Lehtivuori, H. Takala, A. J. Hughes, M. Panman, M. Hoernke, S. Niebling, L. Henry, R. Henning, I. Kosheleva, V. Chukharev, N. V. Tkachenko, A. Menzel, G. Newby, D. Khakhulin, M. Wulff, J. A. Ihalainen, S. Westenhoff, *Sci. Adv.* **2016**, 2, e1600920.
- [45] J. G. Kim, S. Muniyappan, K. Y. Oang, T. W. Kim, C. Yang, K. H. Kim, J. Kim, H. Ihee, *Struct. Dyn.* **2016**, 3, 023610.
- [46] T. W. Kim, C. Yang, Y. Kim, J. G. Kim, J. Kim, Y. O. Jung, S. Jun, S. J. Lee, S. Park, I. Kosheleva, R. Henning, J. J. van Thor, H. Ihee, *Phys. Chem. Chem. Phys.* **2016**, 18, 8911.
- [47] K. Haldrup, A. O. Dohn, M. L. Shelby, M. W. Mara, A. B. Stickrath, M. R. Harpham, J. Huang, X. Zhang, K. B. Møller, A. Chakraborty, F. N. Castellano, D. M. Tiede, L. X. Chen, *J. Phys. Chem. A* **2016**, 120, 7475.
- [48] D. Rimmerman, D. Leshchev, D. J. Hsu, J. Hong, I. Kosheleva, L. X. Chen, *J. Phys. Chem. Lett.* **2017**, 8, 4413.
- [49] O. Berntsson, R. P. Diensthuber, M. R. Panman, A. Bjorling, E. Gustavsson, M. Hoernke, A. J. Hughes, L. Henry, S. Niebling, H. Takala, J. A. Ihalainen, G. Newby, S. Kerruth, J. Heberle, M. Liebi, A. Menzel, R. Henning, I. Kosheleva, A. Moglich, S. Westenhoff, *Nat. Commun.* **2017**, 8, 284.
- [50] C. W. Ahn, H. Ki, J. Kim, J. Kim, S. Park, Y. Lee, K. H. Kim, Q. Kong, J. Moon, M. N. Pedersen, M. Wulff, H. Ihee, *J. Phys. Chem. Lett.* **2018**, 9, 647.
- [51] Y. Kim, P. Ganesan, J. Jo, S. O. Kim, K. Thamilselvan, H. Ihee, *J. Phys. Chem. B* **2018**, 122, 4513.
- [52] D. Leshchev, T. C. B. Harlang, L. A. Fredin, D. Khakhulin, Y. Liu, E. Biasin, M. G. Laursen, G. E. Newby, K. Haldrup, M. M. Nielsen, K. Wärnmark, V. Sundström, P. Persson, K. S. Kjaer, M. Wulff, *Chem. Sci.* **2018**, 9, 405.
- [53] D. Rimmerman, D. Leshchev, D. J. Hsu, J. Hong, B. Abraham, R. Henning, I. Kosheleva, L. X. Chen, *J. Phys. Chem. B* **2018**, 122, 5218.
- [54] C. Yang, M. Choi, J. G. Kim, H. Kim, S. Muniyappan, S. Nozawa, S. I. Adachi, R. Henning, I. Kosheleva, H. Ihee, *Int. J. Mol. Sci.* **2018**, 19, 19.
- [55] E. H. Choi, D.-S. Ahn, S. Park, C. Kim, C. W. Ahn, S. Kim, M. Choi, C. Yang, T. W. Kim, H. Ki, J. Choi, M. N. Pedersen, M. Wulff, J. Kim, H. Ihee, *J. Phys. Chem. Lett.* **2019**, 10, 1279.
- [56] D. J. Heyes, S. J. O. Hardman, M. N. Pedersen, J. Woodhouse, E. De La Mora, M. Wulff, M. Weik, M. Cammarata, N. S. Scrutton, G. Schirò, *Commun. Biol.* **2019**, 2, 1.
- [57] D. J. Hsu, D. Leshchev, D. Rimmerman, J. Hong, M. S. Kelley, I. Kosheleva, X. Y. Zhang, L. X. Chen, *Chem. Sci.* **2019**, 10, 9788.
- [58] D. Khakhulin, L. M. Lawson Daku, D. Leshchev, G. E. Newby, M. Jarenmark, C. Bressler, M. Wulff, S. E. Canton, *Phys. Chem. Chem. Phys.* **2019**, 21, 9277.
- [59] D. Leshchev, D. Khakhulin, G. Newby, H. Ki, H. Ihee, M. Wulff, *J. Chem. Phys.* **2019**, 151, 054310.
- [60] S. Park, J. Choi, H. Ki, K. H. Kim, K. Y. Oang, H. Roh, J. Kim, S. Nozawa, T. Sato, S.-I. Adachi, J. Kim, H. Ihee, *J. Chem. Phys.* **2019**, 150, 224201.
- [61] D. Rimmerman, D. Leshchev, D. J. Hsu, J. Hong, B. Abraham, R. Henning, I. Kosheleva, L. X. Chen, *J. Phys. Chem. B* **2016**, 123, 2016.
- [62] H. Ki, S. Park, S. Eom, J. Gu, S. Kim, C. Kim, C. W. Ahn, M. Choi, S. Ahn, D. S. Ahn, J. Choi, M. H. Baik, H. Ihee, *Int. J. Mol. Sci.* **2020**, 21, 21.
- [63] H. Kim, J. G. Kim, S. Muniyappan, T. W. Kim, S. J. Lee, H. Ihee, *J. Phys. Chem. B* **2020**, 124, 1550.
- [64] T. W. Kim, S. J. Lee, J. Jo, J. G. Kim, H. Ki, C. W. Kim, K. H. Cho, J. Choi, J. H. Lee, M. Wulff, Y. M. Rhee, H. Ihee, *Proc. Natl. Acad. Sci. U. S. A.* **2020**, 117, 14996.
- [65] M. Choi, J. G. Kim, S. Muniyappan, H. Kim, T. W. Kim, Y. Lee, S. J. Lee, S. O. Kim, H. Ihee, *Chem. Sci.* **2021**, 12, 8207.

- [66] S. J. Lee, Y. Kim, T. W. Kim, C. Yang, K. Thamilselvan, H. Jeong, J. Hyun, H. Ihee, *Cell Rep.* **2021**, *2*, 100512.
- [67] D. Arnlund, L. C. Johansson, C. Wickstrand, A. Barty, G. J. Williams, E. Malmerberg, J. Davidsson, D. Milathianaki, D. P. DePonte, R. L. Shoeman, D. Wang, D. James, G. Katona, S. Westenhoff, T. A. White, A. Aquila, S. Bari, P. Berntsen, M. Bogan, T. B. van Driel, R. B. Doak, K. S. Kjær, M. Frank, R. Fromme, I. Grotjohann, R. Henning, M. S. Hunter, R. A. Kirian, I. Kosheleva, C. Kupitz, M. Liang, A. V. Martin, M. M. Nielsen, M. Messerschmidt, M. M. Seibert, J. Sjöhamn, F. Stellato, U. Weierstall, N. A. Zatsepin, J. C. H. Spence, P. Fromme, I. Schlichting, S. Boutet, G. Groenhof, H. N. Chapman, R. Neutze, *Nat. Methods* **2014**, *11*, 923.
- [68] S. E. Canton, K. S. Kjær, G. Vankó, T. B. van Driel, S.-I. Adachi, A. Bordage, C. Bressler, P. Chabera, M. Christensen, A. O. Dohn, A. Galler, W. Gawelda, D. Gosztola, K. Haldrup, T. Harlang, Y. Liu, K. B. Møller, Z. Németh, S. Nozawa, M. Pápai, T. Sato, T. Sato, K. Suarez-Alcantara, T. Togashi, K. Tono, J. Uhlrig, D. A. Vithanage, K. Wärnmark, M. Yabashi, J. Zhang, V. Sundström, M. M. Nielsen, *Nat. Commun.* **2015**, *6*, 6359.
- [69] M. Levantino, G. Schirò, H. T. Lemke, G. Cottone, J. M. Glownia, D. Zhu, M. Chollet, H. Ihee, A. Cupane, M. Cammarata, *Nat. Commun.* **2015**, *6*, 6772.
- [70] E. Biasin, T. B. van Driel, K. S. Kjaer, A. O. Dohn, M. Christensen, T. Harlang, P. Chabera, Y. Liu, J. Uhlrig, M. Papai, Z. Nemeth, R. Hartsock, W. Liang, J. Zhang, R. Alonso-Mori, M. Chollet, J. M. Glownia, S. Nelson, D. Sokaras, T. A. Assefa, A. Britz, A. Galler, W. Gawelda, C. Bressler, K. J. Gaffney, H. T. Lemke, K. B. Møller, M. M. Nielsen, V. Sundstrom, G. Vanko, K. Warnmark, S. E. Canton, K. Haldrup, *Phys. Rev. Lett.* **2016**, *117*, 013002.
- [71] J. G. Kim, S. Nozawa, H. Kim, E. H. Choi, T. Sato, T. W. Kim, K. H. Kim, H. Ki, J. Kim, M. Choi, Y. Lee, J. Heo, K. Y. Oang, K. Ichianagi, R. Fukaya, J. H. Lee, J. Park, I. Eom, S. H. Chun, S. Kim, M. Kim, T. Katayama, T. Togashi, S. Owada, M. Yabashi, S. J. Lee, S. Lee, C. W. Ahn, D.-S. Ahn, J. Moon, S. Choi, J. Kim, T. Joo, J. Kim, S.-I. Adachi, H. Ihee, *Nature* **2020**, *582*, 520.
- [72] K. H. Kim, A. Späh, H. Pathak, C. Yang, S. Bonetti, K. Amann-Winkel, D. Mariedahl, D. Schlesinger, J. A. Sellberg, D. Mendez, G. van der Schot, H. Y. Hwang, J. Clark, O. Shigeki, T. Tadashi, Y. Harada, H. Ogasawara, T. Katayama, A. Nilsson, F. Perakis, *Phys. Rev. Lett.* **2020**, *125*, 076002.
- [73] E. Biasin, Z. W. Fox, A. Andersen, K. Ledbetter, K. S. Kjær, R. Alonso-Mori, J. M. Carlstad, M. Chollet, J. D. Gaynor, J. M. Glownia, K. Hong, T. Kroll, J. H. Lee, C. Liekhus-Schmaltz, M. Reinhard, D. Sokaras, Y. Zhang, G. Doumy, A. M. March, S. H. Southworth, S. Mukamel, K. J. Gaffney, R. W. Schoenlein, N. Govind, A. A. Cordones, M. Khalil, *Nat. Chem.* **2021**, *13*, 343.
- [74] E. H. Choi, J. G. Kim, J. Kim, H. Ki, Y. Lee, S. Lee, K. Yoon, J. Kim, J. Kim, H. Ihee, *Nat. Commun.* **2021**, *12*, 4732.
- [75] H. Kim, J. G. Kim, T. W. Kim, S. J. Lee, S. Nozawa, S.-I. Adachi, K. Yoon, J. Kim, H. Ihee, *Chem. Sci.* **2021**, *12*, 2114.
- [76] M. E. Reinhard, M. W. Mara, T. Kroll, H. Lim, R. G. Hadt, R. Alonso-Mori, M. Chollet, J. M. Glownia, S. Nelson, D. Sokaras, K. Kunnus, T. B. van Driel, R. W. Hartsock, K. S. Kjaer, C. Weninger, E. Biasin, L. B. Gee, K. O. Hodgson, B. Hedman, U. Bergmann, E. I. Solomon, K. J. Gaffney, *Nat. Commun.* **2021**, *12*, 12.
- [77] A. Plech, V. Kotaidis, K. Istomin, M. Wulff, *J. Synchrotron Radiat.* **2007**, *14*, 288.
- [78] T. K. Kim, J. H. Lee, M. Wulff, Q. Kong, H. Ihee, *ChemPhysChem* **2009**, *10*, 2915.
- [79] H. Ihee, M. Wulff, J. Kim, S.-I. Adachi, *Int. Rev. Phys. Chem.* **2010**, *29*, 453.
- [80] J. Kim, K. H. Kim, J. H. Lee, H. Ihee, *Acta Cryst. A* **2010**, *66*, 270.
- [81] J. H. Lee, H. Ihee, *Struct. Chem.* **2010**, *21*, 37.
- [82] K. H. Kim, J. H. Lee, J. Kim, S. Nozawa, T. Sato, A. Tomita, K. Ichianagi, H. Ki, J. Kim, S.-I. Adachi, H. Ihee, *Phys. Rev. Lett.* **2013**, *110*, 165505.
- [83] K. H. Kim, J. Kim, J. H. Lee, H. Ihee, *Struct. Dyn.* **2014**, *1*, 011301.
- [84] J. Kim, K. H. Kim, K. Y. Oang, J. H. Lee, K. Hong, H. Cho, N. Huse, R. W. Schoenlein, T. K. Kim, H. Ihee, *Chem. Commun.* **2016**, *52*, 3734.
- [85] K. H. Kim, J. G. Kim, K. Y. Oang, T. W. Kim, H. Ki, J. Jo, J. Kim, T. Sato, S. Nozawa, S.-I. Adachi, H. Ihee, *Struct. Dyn.* **2016**, *3*, 043209.
- [86] Y. Lee, J. G. Kim, S. J. Lee, S. Muniyappan, T. W. Kim, H. Ki, H. Kim, J. Jo, S. R. Yun, H. Lee, K. W. Lee, S. O. Kim, M. Cammarata, H. Ihee, *Nat. Commun.* **2021**, *12*, 3677.
- [87] H.-J. Kim, S. Cho, J. S. Park, *Bull. Korean Chem. Soc.* **2015**, *36*, 2740.
- [88] J. H. Kim, B. Min, Y. D. Yun, H. J. Choi, K. S. Jin, *Bull. Korean Chem. Soc.* **2020**, *41*, 1052.
- [89] J. G. Kim, K. H. Kim, K. Y. Oang, T. W. Kim, H. Ki, J. Jo, J. Kim, T. Sato, S. Nozawa, S.-I. Adachi, H. Ihee, *J. Phys. B: At., Mol. Opt. Phys.* **2015**, *48*, 244005.
- [90] K. H. Kim, J. G. Kim, S. Nozawa, T. Sato, K. Y. Oang, T. W. Kim, H. Ki, J. Jo, S. Park, C. Song, T. Sato, K. Ogawa, T. Togashi, K. Tono, M. Yabashi, T. Ishikawa, J. Kim, R. Ryoo, J. Kim, H. Ihee, S.-I. Adachi, *Nature* **2015**, *518*, 385.
- [91] J. Kim, J. G. Kim, H. Ki, C. W. Ahn, H. Ihee, *J. Synchrotron Radiat.* **2020**, *27*, 633.
- [92] D. Waasmaier, A. Kirfel, *Acta Cryst. A* **1995**, *51*, 416.
- [93] K. S. Kjær, T. B. van Driel, J. Kehres, K. Haldrup, D. Khakhulin, K. Bechgaard, M. Cammarata, M. Wulff, T. J. Sørensen, M. M. Nielsen, *Phys. Chem. Chem. Phys.* **2013**, *15*, 15003.
- [94] H. Ihee, B. M. Goodson, R. Srinivasan, V. A. Lobastov, A. H. Zewail, *J. Phys. Chem. A* **2002**, *106*, 4087.
- [95] B. N. Figgis, B. W. Skelton, A. H. White, *Aust. J. Chem.* **1978**, *31*, 57.
- [96] J. Cao, H. Ihee, A. H. Zewail, *Proc. Natl. Acad. Sci. U. S. A.* **1999**, *96*, 338.
- [97] H. Ihee, J. Cao, A. H. Zewail, *Angew. Chem., Int. Ed.* **2001**, *40*, 1532.
- [98] H. Ihee, J. S. Feenstra, J. Cao, A. H. Zewail, *Chem. Phys. Lett.* **2002**, *353*, 325.

**How to cite this article:** H. Jeong, H. Ki, J. G. Kim, J. Kim, Y. Lee, H. Ihee, *Bull. Korean Chem. Soc* **2022**, *43*(3), 376. <https://doi.org/10.1002/bkcs.12494>